



Electrical Propagation of Vasodilatory Signals in Capillary Networks

Pilhwa Lee¹

Received: 12 November 2019 / Accepted: 9 September 2020 / Published online: 23 September 2020
© Society for Mathematical Biology 2020

Abstract

We have developed a computational model to study electrical propagation of vasodilatory signals and arteriolar regulation of blood flow depending on the oxygen tension and agonist distribution in the capillary network. The involving key parameters of endothelial cell-to-cell electrical conductivity and plasma membrane area per unit volume were calibrated with the experimental data on an isolated endothelial tube of mouse skeletal feeding arteries. We have estimated the oxygen saturation parameters in terms of erythrocyte ATP release from the data of a left anterior descending coronary blood perfusion of dog. Regarding the acetylcholine-induced upstream conduction, our model shows that spatially uniform superfusion of acetylcholine attenuates the electrical signal propagation, and blocking calcium-activated potassium channels suppresses that attenuation. On the other hand, a local infusion of acetylcholine induces enhanced electrical propagation that corresponds to physiological relevance. Integrating the electrophysiology of endothelial tube and the electrophysiology/mechanics of a lumped arteriole, we show mechanistically that endothelial purinergic oxygen sensing of ATP released from erythrocytes and local infusion of acetylcholine are individually effective to induce vasodilatory signals to regulate blood flow in arterioles. We have recapitulated the upstream vasomotion in arterioles from the elevated oxygen tension in the downstream capillary domain. This study is a foundation for characterizing effective pharmaceutical strategies for ascending vasodilation and oxygenation.

Keywords Vasodilation · Calcium-activated potassium channel · Purinergic signal · ATP hypothesis

✉ Pilhwa Lee
jpilpo77@gmail.com

¹ Molecular and Integrative Physiology, University of Michigan, Ann Arbor, USA

1 Introduction

We investigate the influence of vasodilatory signals in the electrical propagation in the endothelium of microvasculature and dilation in the upstream arterioles. Blood flow regulation in the microcirculation is crucial for maintaining relevant pressure tone and tissue oxygenation. In arterioles and capillary microvasculature, the downstream signaling of oxygen demand or hypertension induces upstream conducted vasodilation (Bagher and Segal 2011). The upstream propagation of electrical signals in the microvasculature is activated by exercise at a healthy state (Duncker and Bache 2008). However, it may cause dysfunction at disease states such as diabetes (Fitzgerald et al. 2005; Park et al. 2008; Bender et al. 2009), obesity (Haddock et al. 2011), and hypertension (Brahler et al. 2009).

Microvascular dilation is regulated by agonists such as cholinergic acetylcholine (ACh) (Doyle and Duling 1997), plasma ATP (Ellsworth 2000), and also via sympathetic control of β -adrenergic signaling (Feigl 1998). Dilation in coronary arterioles is also flow-dependent (Kuo et al. 1990). We target the response to agonists of ACh and plasma ATP through a couple of steps to increase cytosolic calcium concentration (Chen and Cheung 1992; Communi et al. 2000; Raqeeb et al. 2011) or directly to a pharmaceutical drug of SK_{Ca} and IK_{Ca} (small and intermediate conductance Ca^{2+} activated K^+ channels) opener, NS309 (6,7-dichloro-1H-indole-2,3-dione 3-oxime).

The mechanism of vasodilation by propagated electrical signals is mainly processed through the following steps: (1) In the initiation, the vasodilatory agonists increase cytosolic calcium concentration via G-protein coupled receptors and IP_3 induced calcium release from the endoplasmic reticulum (ER). (2) The elevated calcium hyperpolarizes the endothelial cell (EC) membrane via SK_{Ca} and IK_{Ca} channels (Stankevicius et al. 2011). The hyperpolarization in the downstream is conducted to upstream through endothelial gap junction channels (GJCs) (Goto et al. 2002; Diep et al. 2005; Schmidt et al. 2008). (3) The hyperpolarization in the EC layer is transmitted to the smooth muscle cell (SMC) layer via the myoendothelial junction. It closes L-type calcium channels lowering the influx of calcium ions (Kapela et al. 2009). (4) The elevated calcium in the EC also produces nitric oxide (NO), and the increased NO is transported to the SMC layer to decrease calcium through the cGMP pathway (Kapela et al. 2009).

We study the following questions to characterize the vasodilatory signal propagation in model capillary networks: (1) How far can a localized hyperpolarized signal propagate? (2) What are the conditions under which a physiologically significant depolarization (tens of millivolts) occurs (3) How influential are endogenous agonists and pharmaceutical drugs on the upstream vasodilation? To address these questions, we have developed a mono-domain based endothelial tube model with an endothelial cell model modified from Silva et al. (2007). Next, we integrated the electrophysiology of the endothelial tube and the electrophysiology/mechanics of a lumped arteriole (i.e., endothelial cells coupled to smooth muscles via myoendothelial junctions) as shown in Fig. 1b.

We realized the electrical signal propagation speed about 2.5 mm/s and the electrical length constant (λ) about 1.1 mm that are consistent with the experimental data (Segal and Duling 1986). In the model simulation, λ decreases with more ACh/NS309

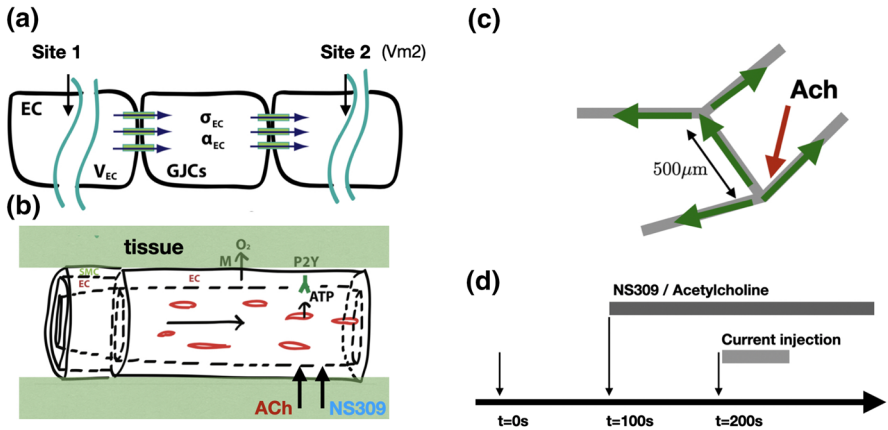


Fig. 1 The EC tube model for oxygen sensing coupled to a lumped arteriole. **a** The electrophysiology of endothelium at the cellular level is based on the model of Silva et al. (2007). The SK_{Ca}/IK_{Ca} dependency on NS309 is newly included. IP_3 generation rates depend on infused ACh or plasma ATP levels. Cell-cell electrical interaction is through non-selective gap junctions. In the mono-domain formulation, we have primarily estimated the electrical conductivity in the EC layer (σ_{EC}) and the EC membrane area per unit volume (α_{EC}). The electrical potential in the intracellular domain is defined as V_{EC} , the same as the membrane voltage V_m . V_{m2} is the V_m at Site 2 with the distance s from Site 1. **b** The pre-capillary arteriole is represented by the electrophysiology model of endothelial cells and the electrophysiology and mechanics model of myogenic smooth muscle (Carlson and Beard 2011). The oxygen consumption rate of the tissue where the capillary network is immersed is denoted by M . **c** Schematic configuration of five capillary endothelial tubes with each tube length of $500 \mu m$. From a local injection of ACh, the electrical hyperpolarization is propagated in the directions indicated by green arrows. **d** NS309/ACh is infused from $t = 100$ sec, and the current is applied from $t = 200$ to 202 s for characterizing the EC tube model (Color figure online)

application when the dilators are uniformly superfused. In contrast, a local application of the agonists makes the electrical signals propagate further, and indeed this captures some physiological conditions for different effects of ACh to the electrical propagation (Emerson et al. 2002; Behringer and Segal 2012). The integrated model shows the physiological vasodilatory response from low oxygen tension in the downstream observed in canine coronary blood flow (Farias et al. 2005) and cholinergic signals observed in skeletal muscle of hamster (Bagher and Segal 2011). Here, the model oxygen sensing is assumed to be from the purinergic binding of ATP released from erythrocytes (Ellsworth 2000) and affects IP_3 generation rates in the endothelium (Communi et al. 2000; Raqeeb et al. 2011).

We expect the proposed endothelial tube model in the capillary network to provide a foundation for further study of blood flow regulation from vasodilatory signals in pathophysiological states such as ischemic hypoxia, hypertension, and metabolic syndrome as well as therapeutic and preclinical drug screening.

2 Methods

2.1 Mono-domain Capillary Network

Mathematical formulation The electrical conduction in the capillary network is represented by a mono-domain formulation, i.e., the electrical potential at the extracellular domain surrounding the capillary networks is assumed to be constant or grounded, and the conduction of the electrical potential of endothelial cells in the capillary networks is formulated by a cell-to-cell electrical conductivity. In the mono-domain formulation, the electrical current in the EC layer is represented by the electrical conductivity σ_{EC} as follows:

$$j_{EC} = -\sigma_{EC} \frac{\partial V_{EC}}{\partial s}, \quad (1)$$

where V_{EC} is the electrical potential of the endothelial layer, and s is the Lagrangian coordinate along the EC layer. In the continuity equation for electrical endothelial currents, the current from membrane voltage change in time with membrane capacitance per unit area C_m , membrane ionic currents I_{EC}^i , and the external current injection $I_{INJECTION}$ induce a gradient in the electrical currents through the gap junction:

$$\frac{\partial j_{EC}}{\partial s} = -\alpha_{EC} \left(C_m \frac{\partial V_m}{\partial t} + \sum_i I_{EC}^i + I_{INJECTION} \right), \quad (2)$$

where V_m (membrane voltage) is the same as V_{EC} , with the extracellular domain grounded as zero. We explicitly represent the transmitted electrical currents from the extracellular domain to the EC layer with I_{EC}^i for i^{th} ionic species (Na^+ , K^+ , Cl^- , Ca^{2+}). The scaling factor α_{EC} is the endothelial plasma membrane area per unit volume. The cellular solute/ionic dynamics is the same as the mathematical formulation in Silva et al. (2007) for ionic currents and transporter/exchangers:

$$\frac{\partial c_i}{\partial t} = f_i(c_j, V_m), \quad (3)$$

with the ionic currents from inward rectifier potassium channels (Kir), calcium-activated potassium channels (KCa: SK_{Ca} and IK_{Ca}) calcium-activated chloride channels (CaCC), voltage-regulated anion channels (VRAC), store-operated cation channels (SOC), non-selective cation channels (NSC), sodium-calcium exchangers (NCX), sodium-potassium exchangers (NaK), sodium-potassium-chloride ($\text{Na}^+/\text{K}^+/\text{2Cl}^-$) co-transporters, plasma membrane calcium ATPase pumps (PMCA).

In brevity, the dominant K^+ conductance is by Kir channels, and this is considered key for resting V_m regulation. KCa channels are activated to induce hyperpolarization as cytosolic calcium concentration elevates. CaCC can function for calcium inflow by membrane depolarization. This is in feedback control loops with the action of KCa channels. VRAC channels are constitutively active and play an important role in determining their resting V_m . SOC channels sustain elevated cytosolic calcium levels

and a major EC calcium influx pathway during agonist stimulation. NSC current contributes to the balance of Na^+ , K^+ , Ca^{2+} , and provides an alternative pathway for calcium entry into the cytosol. The NCX, an electrogenic transporter of Na^+ and Ca^{2+} , is found in EC and included in the model. The NaK pump has been found in various EC types, and it represents the main ionic pump in mammalian cell membranes. The NaKCl co-transporter pivotally involves in the main influx of K^+ , even surpassing the NaK contribution. The PMCA is responsible for determining resting cytosolic calcium levels. See Silva et al. (2007) for the details.

The indirect endogenous agonist ACh or plasma ATP regulate IP_3 dynamics, and the governing equations of IP_3 are shown as follows:

$$\begin{aligned} \frac{d\text{IP}_3}{dt} &= Q_{\text{GIP}_3} - k_{\text{DIP}_3}[\text{IP}_3], & (4) \\ \frac{dQ_{\text{GIP}_3}}{dt} &= \frac{Q_{\text{GIP}_3\text{SS}} - Q_{\text{GIP}_3}}{\tau_{\text{IP}_3}}, & (5) \end{aligned}$$

where IP_3 is the cytosolic IP_3 concentration, Q_{GIP_3} is the cytosolic IP_3 generation rate, and k_{DIP_3} is the IP_3 degradation rate. $Q_{\text{GIP}_3\text{SS}}$ is the steady-state IP_3 generation rate, and τ_{IP_3} is the time constant for the IP_3 generation rate (Silva et al. 2007). In case the effect of ACh agonist is considered, we changed $Q_{\text{GIP}_3\text{SS}}$ proportional to $[\text{ACh}]$, with 6.6×10^{-8} mM/ms for $[\text{ACh}] = 3 \mu\text{M}$. When oxygen sensing by plasma ATP is treated (Sect. 2.3), $Q_{\text{GIP}_3\text{SS}}$ is proportional to the plasma ATP concentration (C_T), with 13.2×10^{-8} mM/ms for $C_T = 50$ nM.

The model for calcium-activated potassium channels is modified from Silva et al. (2007) with the gating sensitivity to the direct agonist NS309. We formulated the open probability, $P_{o,x}$ with the competitive binding of cytosolic calcium and NS309 based on the data from Behringer and Segal (2012):

$$P_{o,x} = \frac{[\text{Ca}^{2+}]_{\text{in}}^{nX} / K_{X,\text{Ca}_{\text{in}}}^{nX} + [\text{NS309}]^{n\text{NS309}} / K_{X,\text{NS309}}^{n\text{NS309}}}{1 + [\text{Ca}^{2+}]_{\text{in}}^{nX} / K_{X,\text{Ca}_{\text{in}}}^{nX} + [\text{NS309}]^{n\text{NS309}} / K_{X,\text{NS309}}^{n\text{NS309}}}, \quad (6)$$

where X indicates SK_{Ca} or IK_{Ca} channels, and nX and $K_{X,\text{Ca}}$ denote the Hill coefficient and the half-saturation coefficient for calcium. As a whole, most parameters are the same as Silva et al. (2007), and the modified or newly added parameters are listed in Table 1.

In the capillary network, the boundary condition for downstream terminal nodes is $j_{\text{EC}} = 0$ so that the terminal nodes are sealed electrically. On the other hand, boundary conditions for bifurcation nodes are prescribed as $\sum_i j_{\text{EC},i} = 0$ satisfying the conservation of currents.

For the simulation of vasodilation, in the upstream ($s = 0$), we couple the endothelium with the lumped arteriole in the following:

$$\alpha_{\text{SMC}} \left(C_{\text{m}}^{\text{SMC}} \frac{dV_{\text{m}}^{\text{SMC}}}{dt} + \sum_i I_{\text{SMC}}^i + \sum_i I_{\text{EC,SMC}}^i \right) + \frac{\partial j_{\text{EC}}}{\partial s} \Big|_{s=0} = 0, \quad (7)$$

Table 1 Endothelial parameters

Symbol	Definition	Value
σ_{EC}	EC electrical conductivity	1.3×10^{-15} S cm (estimated)
α_{EC}	EC plasma membrane area per unit volume	0.32/cm (estimated)
C_m	Membrane capacitance per unit area	0.02 pF (estimated)
$g_{SK_{Ca}}$	Maximum SK_{Ca} conductance	0.1534 nS (Silva et al. 2007)
$g_{IK_{Ca}}$	Maximum IK_{Ca} conductance	0.4254 nS (Silva et al. 2007)
K_{NS309}	Half saturation coefficient for NS309	1.0 μ M (estimated)
n_{NS309}	Hill coefficient for NS309	1.3 (estimated)

where V_m^{SMC} is the membrane voltage, α_{SMC} is the plasma membrane area per unit volume, and C_m^{SMC} is the membrane capacitance per unit area of the SMC. The governing equations and parameters for SMC ion channels and the associated currents (I_{SMC}^i) are fully from the model of Carlson and Beard (2011), and the details are referred to the cited paper. Those for myoendothelial junctions ($I_{EC,SMC}^i$) are from Kapela et al. (2009).

Parameterization of the mono-domain model To parameterize the mono-domain model, we used the electrical propagation in the endothelial tube from the experimental data of skeletal muscle (Behringer and Segal 2012). As described in the simulation protocol (Fig. 1c; Sect. 2.4), SK_{Ca} and IK_{Ca} channels are inactivated until $t = 100$ s, and then activated from $t = 100$ s. The direct activation of SK_{Ca}/IK_{Ca} channels is realized by treating the pharmacological drug NS309 1 μ M, and the indirect activation by the endogenous agonist ACh 3 μ M. The current is injected at Site 1 from $t = 200$ to 202 s (Fig. 1a). Figure 2a, c shows the simulated time courses of V_m at Site 2 (V_{m2}) with the distance $s = 500 \mu$ m from Site 1 when NS309 and ACh agonists are superposed uniformly through the entire EC tube domain, respectively. When SK_{Ca} and IK_{Ca} channels are activated, the endothelial tube is hyperpolarized from the resting state (about -20 mV) to -60 mV. In control with SK_{Ca} and IK_{Ca} channels inactivated before $t = 100$ s, the endothelial tube stays in the initial resting potential. The maximum peaks of ΔV_m from current injection are more significant compared to the responses in hyperpolarized states. Figure 2b, d corresponds to the experimental data from the application of NS309 and ACh (Behringer and Segal 2012).

Figure 3 shows the comparison between the experimental data of electrical signal propagation on the EC tube and the model simulation with two primary estimated parameters, the endothelial electrical conductivity (σ_{EC}) and the endothelial plasma membrane area per unit volume (α_{EC}). We have used the electrical propagation data with activated/inactivated SK_{Ca} and IK_{Ca} channels for the parameterization. The data used in the parameterization is ΔV_m , the maximum difference of membrane voltage before and after membrane depolarization with current injection. Those ΔV_m are collected from $s = 50, 500, 1000,$ and 1500μ m at Site 2. We have applied a gradient descent algorithm for minimizing the squared error between model-simulated ΔV_m and the corresponding experimental data (Fig. 3a–c). This is iteratively done, first for σ_{EC} , and next for α_{EC} until there comes a convergence with relative tolerance 10^{-5} . The

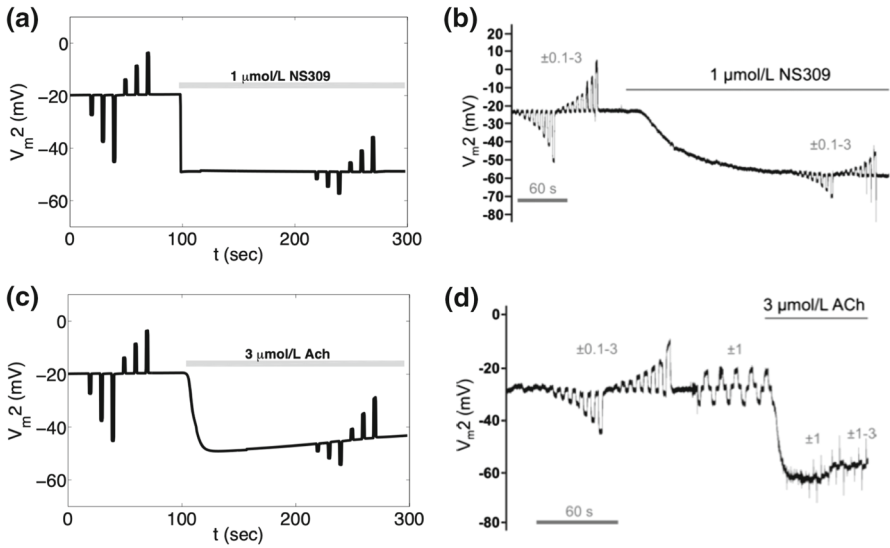


Fig. 2 Time course of V_{m2} with NS309 and ACh application. **a** Time course of V_m at $s = 500 \mu\text{m}$ (V_{m2}) with $1 \mu\text{M}$ NS309 from $t = 100 \text{ s}$. The pharmaceutical dilator NS309 directly activates $\text{SK}_{\text{Ca}}/\text{IK}_{\text{Ca}}$ channels and hyperpolarizes membrane voltage to about -60 mV and attenuates the response from a current injection. The EC tube model is simulated with the current injection at Site 1 ($\pm 1, 2, 3 \text{ nA}$) before and after NS309 treatment. **b** The corresponding experiment from Behringer and Segal (2012, Figure 2A). **c** Time course of V_m at $s = 500 \mu\text{m}$ (V_{m2}) with ACh $3 \mu\text{M}$ from $t = 100 \text{ s}$. ACh indirectly activates $\text{SK}_{\text{Ca}}/\text{IK}_{\text{Ca}}$ channels via G-protein coupled receptors and hyperpolarizes the membrane voltage to about -60 mV and attenuates electrical conduction. The endothelial tube model is simulated with a current injection at Site 1 ($\pm 1, 2, 3 \text{ nA}$) before and after ACh infusion. **d** The corresponding experiment from Behringer and Segal (2012, Figure 7A)

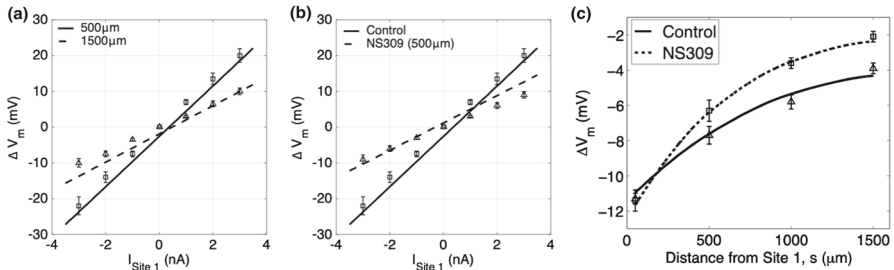


Fig. 3 EC tube parameterization and validation. The mono-domain parameters ($\sigma_{\text{EC}}, \alpha_{\text{EC}}$) are parameterized with the experimental data in Behringer and Segal (2012). The experimental data are shown with error bars. **a** ΔV_m at $s = 500$ and $1500 \mu\text{m}$ with a current injection at Site 1 ($\pm 1, 2, 3 \text{ nA}$). The solid and dotted lines are fitted from simulations with the estimated parameters ($\sigma_{\text{EC}}, \alpha_{\text{EC}}$) at $s = 500$ and $1500 \mu\text{m}$, respectively. **b** ΔV_m at $s = 500 \mu\text{m}$ in control (no NS309) or the application of $1 \mu\text{M}$ NS309. The solid and dotted lines are fitted from simulations with the estimated parameters ($\sigma_{\text{EC}}, \alpha_{\text{EC}}$) without and with NS309, respectively. **c** ΔV_m at $s = 50, 500, 1000$, and $1500 \mu\text{m}$ in control (no NS309) or the application of $1 \mu\text{M}$ NS309. The solid and dotted curves (polynomials with degree of 4) are fitted from simulations with the estimated parameters ($\sigma_{\text{EC}}, \alpha_{\text{EC}}$) without and with NS309, respectively

parameters of C_m and K_{NS309}/n_{NS309} are similarly fitted from the data of Behringer and Segal (2012).

Figure 3a shows the linear curve fitting with the graded current injection ($\pm 1, 2, 3$ nA) at $s = 500$ and $1500 \mu\text{m}$ in control. The solid curve is from simulated ΔV_m at $s = 500 \mu\text{m}$, and the square data points/error bars are from experiments. The dotted curve is from simulated ΔV_m at $s = 1500 \mu\text{m}$, and the triangle data points/error bars are from experiments. With the electrical propagation attenuation, the slope of the curves has decreased. Figure 3b demonstrates the linear curve fitting with ΔV_m at the same position $s = 500 \mu\text{m}$ with NS309 ($1 \mu\text{M}$) and control (before NS309 treatment). The solid curve is from simulated ΔV_m at the control, and the square data points/error bars are from experiments. The dotted curve is from the simulated ΔV_m with NS309 treatment, and the square data points/error bars are from experiments. With the hyperpolarization of the EC tube, the slope of the curves has decreased. In Fig. 3c, we fitted the electrical signal attenuation with different current injections (1 nA for control, 2 nA for NS309) from Site 2 with a few distances, $s = 50, 500, 1000,$ and $1500 \mu\text{m}$. The solid curve is from simulated ΔV_m at the control, and the triangle data points/error bars are from experiments. The dotted curve is from the simulated ΔV_m with NS309 treatment, and the square data points/error bars are from experiments. The parameterized EC tube model satisfies the electrical length constants quantitatively in the control and NS309 application.

2.2 Blood Flow Perfusion

The total vessel wall stress, σ_{total} in the lumped arteriole is given by

$$\sigma_{\text{total}} = \sigma_{\text{pass}}(D) + \text{Act}([\text{Ca}^{2+}]_{\text{SMC}}) \cdot \sigma_{\text{act}}^{\text{max}}(D), \quad (8)$$

where σ_{pass} and $\sigma_{\text{act}}^{\text{max}}$ are the nonlinear passive stress and the maximally active stress in terms of the vessel diameter D (Carlson and Beard 2011). Act is the state variable for the smooth muscle activation in terms $[\text{Ca}^{2+}]_{\text{SMC}}$, determined by the cross-bridge dynamics in the SMC (Hai and Murphy 1988). The total vessel wall stress is given by the Law of Laplace as follows:

$$\sigma_{\text{total}} = \frac{PD}{2\delta_{\text{wall}}}, \quad (9)$$

where P is the intraluminal pressure, and δ_{wall} is the vessel wall thickness. The blood flow perfusion is determined by the diameter of the lumped pre-capillary arteriole, assuming that the pressure gradient is constant. With the equilibrium of vessel mechanics from Eqs. (8) and (9), the arteriolar diameter D is determined in terms of the SMC calcium concentration $[\text{Ca}^{2+}]_{\text{SMC}}$ and the prescribed pressure P :

$$D = D([\text{Ca}^{2+}]_{\text{SMC}}, P). \quad (10)$$

The overall parameters are from Carlson and Beard (2011), and the main parameters are listed in Table 2. In small resistance vessels, the perfusion flow rate follows the

Table 2 Smooth muscle and blood perfusion parameters

Symbol	Definition	Value
P	Arterioles transmural pressure	100 mmHg
α_{SMC}	SMC plasma membrane area per unit volume	0.32/cm (estimated as the same as α_{EC})
C_m	Membrane capacitance per unit area	25 pF (Kapela et al. 2008)
F_0	Perfusion constant	0.7 mL/min/g
D_0	Baseline diameter	90 μ m

Poiseuille flow:

$$F = F_0 \left(\frac{D}{D_0} \right)^4, \tag{11}$$

where the baseline diameter D_0 and the corresponding perfusion flow rate F_0 are prescribed for the condition without active force. The flow rate is proportional to the 4th power of the arterial diameter, very sensitive to the change of diameter when the pressure gradient is constant.

2.3 Oxygen Sensing and Erythrocyte ATP Release Model

The oxygen saturation S in a capillary of length L is linearly dependent on the steady-state oxygen consumption rate M :

$$S(x) = S_a - \frac{M}{FH_dC_a} \frac{x}{L}, \tag{12}$$

where S_a is the oxygen saturation in the arteriole, H_d is the hematocrit, and C_a is the oxygen-carrying capacity. The Lagrangian coordinate along the EC tube is denoted by x instead of s to prevent the confusion between s and S . The plasma ATP concentration, C_T is governed by transport and production from erythrocytes:

$$\frac{\partial C_T}{\partial t} = -\frac{FL}{V_c} \frac{\partial C_T}{\partial x} + J_0 e^{-S/S_0}, \tag{13}$$

where V_c is the capillary volume density, and F is the perfusion flow rate. Treated similar to Pradhan et al. (2016), $J_0 e^{-S/S_0}$ is the rate of ATP release from erythrocytes into plasma, exponentially decreasing dependent on the oxygen saturation S . The steady-state plasma ATP concentration at $x = L$ is the following:

$$C_T(L) = \frac{V_c J_0}{\alpha FL} e^{-S_a/S_0} (e^{\alpha L} - 1) + C_T(0), \tag{14}$$

where $\alpha = M/(FH_dC_aL)$. The experimental data for the arterial plasma ATP concentration $C_T(0)$, myocardial oxygen consumption rate M , coronary blood flow F ,

Table 3 Oxygen sensing of ATP

Symbol	Definition	Value
C_a	Oxygen carrying capacity	21.5 $\mu\text{L}\cdot\text{O}_2/\text{g}$ (estimated)
S_a	Arterial oxygen saturation	0.96 (Pradhan et al. 2016)
V_C	Capillary volume density	0.04 mL/g (Pradhan et al. 2016)
S_0	ATP generation rate parameter	0.066 (estimated)
J_0	ATP generation rate parameter	110.4 nM/min (estimated)
C_T	ATP concentration in plasma	20.0–60.0 nM (Farias et al. 2005)
M	Oxygen consumption rate	5–100 $\mu\text{L O}_2/\text{g}/\text{min}$ (Farias et al. 2005)
H_d	Hematocrit	~40% (Farias et al. 2005)
$[\text{ATP}]_{\text{init}}$	ATP concentration initial value	40.0 nM

hematocrit H_d , coronary venous plasma ATP concentration $C_T(L)$ are from Table 1 in Farias et al. (2005). By minimizing the least-square error, J_0 , S_0 , and C_a parameters are identified (Table 3).

Ideally, the parameters for electrical conductivity and oxygen saturation for an endothelial tube should be from the same animal and the same circulatory area of vasculature. The electrical conductance lengths of mouse skeletal feeding arteries and coronary artery of dog are about 1.1 and 0.85 mm, respectively (Behringer and Segal 2012; Ito et al. 1980). Since these values are comparable, it is justified to use a combination of these values.

2.4 Simulation Protocol

Parameterization on EC tube The simulation protocol for an isolated EC tube (2 mm) is the following: (i) The direct/indirect activation of SK_{Ca} and IK_{Ca} channels via NS309/ACh agonists is applied from $t = 100$ sec. (ii) From $t = 200$ to 202 s, a current injection of 1 nA is applied at Site 1 (Fig. 1a). (iii) In case ACh is applied locally, the agonist is infused from $s = 100$ to 500 μm along the EC tube and from $t = 100$ to 150 s in time (Fig. 1d). In addition, the external current 1 nA is injected at $s = 250$ μm from $t = 133$ to 136 s.

Capillary network In the model capillary network simulation, we constructed five EC tubular segments (each 500 μm) with two bifurcation nodes, as shown in Fig. 1c. In the local zone of one bifurcation node (Fig. 6a), ACh is infused in the amount of 6 μM for the simulation time. The injection of the current -5 nA is applied for a finite time from $t = 20$ to 28 s locally at a site within the local zone where ACh is infused (Fig. 6b).

Vasodilation with oxygen sensing For the oxygen sensing in the downstream, we focused on the isolated EC tube and applied a range of oxygen consumption rate M (30 to 270 $\mu\text{L}\cdot\text{O}_2/\text{g}/\text{min}$). We reconstructed the electrophysiology and mechanics of smooth muscle cells in the lumped arteriole: membrane voltage V_m , calcium concentration $[\text{Ca}^{2+}]_{\text{in}}$, vessel diameter D , and perfusion flow rate F .

Vasodilation with local ACh infusion To study the local infusion of ACh in the downstream of the EC tube and see the vasodilation in the upstream, we have applied ACh (6, 9, 12, 18, and 24 μM) from 1500 to 2000 μm , and measured the peak dilation and relaxation time of the dilatory response of the lumped arteriole.

2.5 Numerical Methods

We apply an alternating decoupled computation between the electrical signal propagation (Eqs. 1 and 2) for EC and the cellular dynamics of EC/SMC electrophysiology (Eq. 3 and 7) and the SMC vasodilation (Eqs. 8–10). That means, we take time-stepping for the spatial membrane voltage distribution with the cell dynamics and SMC vessel mechanics fixed, whose time-steppings are followed up with the updated $V_m(s)$. We discretized the governing equations, Eqs. (1) and (2) of the spatiotemporal propagation of the electrical potential and the continuity of electrical currents in the bifurcation sites by the backward Euler scheme for time-stepping and a second-order centered differencing in space. After rearrangements, the system of linear equations is solved by the Krylov subspace iteration using PETSc (Balay et al. 1997, 2019a,b). The computation on the cellular solute/ionic transport, Eq. (3), is accelerated along the endothelial tube with parallelized GPU and backward differentiation formula (BDF) using CVODE (Cohen and Hindmarsh 1996). For the determination of the lumped arteriole diameter D from Eqs. (8–10), an iterative Newton method is applied. We have applied absolute and relative tolerances are 10^{-12} and 10^{-8} for those solvers, respectively.

3 Results

Effects of acetylcholine in electrical propagation and calcium dynamics We investigated the effects of ACh in the electrical propagation and calcium dynamics from the parameterized EC tube model. In Fig. 4, we show the spatial distribution of V_m and $[\text{Ca}^{2+}]_{\text{in}}$ without and with ACh. When ACh is not applied, the resting potential stays at around -20 mV , and the cytosolic calcium level is around the baseline 70 nM . As of model validation, the current -3 nA is injected at $s = 1000\ \mu\text{m}$ from $t = 0.0\text{ s}$. The hyperpolarized V_m profile is compared with that from the 1D cable equation (Fig. 4a, red curve):

$$V_m = V_0 e^{-(s-s_0)/\lambda} \quad (15)$$

where V_0 is the membrane voltage at $s_0 = 1000\ \mu\text{m}$, and the electrical length constant, $\lambda = \sqrt{r_m/r_a}$. The membrane resistance, r_m and the axial resistance to current flow, r_a are from Behringer and Segal 2012. In the spatial distribution, V_m is at the peak in the position of current injection ($s = s_0$) and exponentially spreads out. Without ACh, the steady current injection hyperpolarizes the EC tube to around -50 mV within 0.2 s (Fig. 4a, b). cytosolic calcium is elevated to about 130 nM in 20 s .

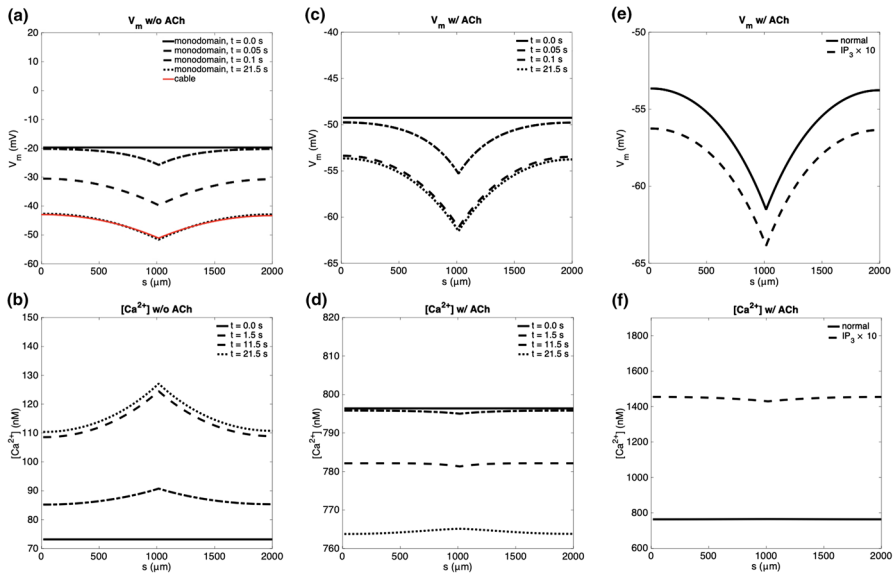


Fig. 4 Mono-domain versus 1D cable equation and the effects of IP_3R overexpression on calcium dynamics. The current -3 nA is injected at $s = 1000$ μm from $t = 0.0$ s. The endothelial layer is most hyperpolarized in the current injected position, and the membrane voltage is exponentially spread out. Accordingly, the cytosolic calcium is elevated with a slower response than V_m . **a** and **b** Without ACh, from the resting potential V_m about -20 mV, the steady current injection hyperpolarizes the EC tube to around -50 mV within 0.2 s. The mono-domain electrical propagation is compared with that of the 1D cable equation (red curve). The involving parameters (λ , r_a) are from Behringer and Segal (2012). The cytosolic calcium is elevated from the baseline level of 70 – 130 nM in 20 s. **c** and **d** With the superfusion of ACh 3 μM for a long time until $t = 0.0$ sec, the EC tube is hyperpolarized to -50 mV, and the membrane is more hyperpolarized to about -62 mV within 2.0 s from the steady current injection -3 nA. At $t = 0.0$ s, the cytosolic calcium is already elevated from IP_3 induced calcium release activated by ACh. From there on, the calcium level is lowered with calcium uptake and IP_3 degradation. **e** and **f** With tenfold overexpression of IP_3R , positive feedback of calcium release from ER is strengthened. As a consequence, the cytosolic calcium gets higher, and the EC tube is more hyperpolarized

When ACh 3 μM is superfused until $t = 0.0$ s, the cytosolic calcium level rises to about 795 μM from IP_3 induced calcium release activated by ACh, and the membrane is hyperpolarized by calcium-activated potassium channels. From there on, the cytosolic calcium level is lowered with calcium uptake and IP_3 degradation. The membrane voltage goes down to about -50 mV, and the membrane is more hyperpolarized to about -62 mV within 2.0 s from the steady current injection -3 nA (Fig. 4c, d). When the positive feedback of calcium release from ER is strengthened with tenfold overexpression of IP_3R , the cytosolic calcium increases, and the EC tube is more hyperpolarized (Fig. 4e, f).

The response of V_m is fast, and V_m gets back to the initial resting potential about -20 mV within 2.5 s after the current injection is terminated at $t = 2.0$ s. In contrast, the calcium response is slow with no change in calcium level at $t = 0.25$ s after the current injection at $t = 0.0$ s. At $t = 2.5$ s, the cytosolic calcium is still recovering in transition whether the EC tube is infused with ACh or not.

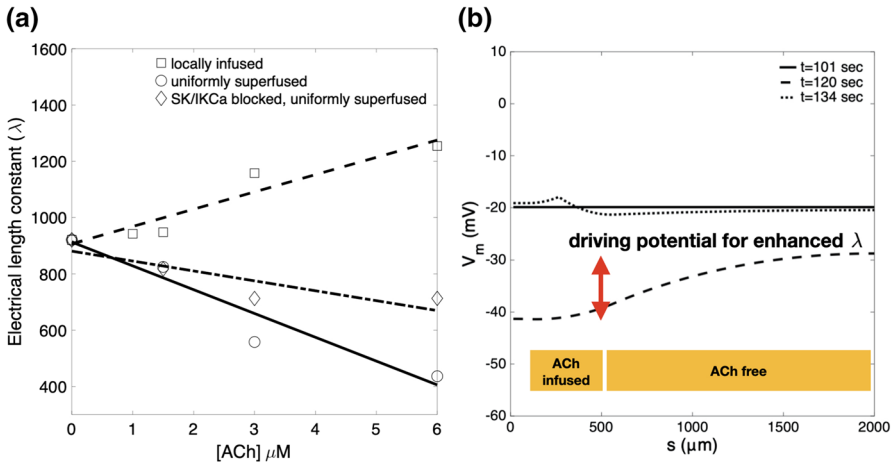


Fig. 5 Electrical length constant versus [ACh]. **a** The steady-state IP_3 generation rate $6.6 \times 10^{-5} \text{ mM/s}$ corresponds to $[\text{ACh}] = 3 \mu\text{M}$ with other values in a linear relationship. The electrical length constant is obtained from ΔV_m at $s = 50, 500, 1000,$ and $1500 \mu\text{m}$. In the solid curve with circle data points, ACh is assumed to be uniformly superfused to the entire EC tube. The dotted curve with square data points represents the electrical propagation with a local ACh infusion from $s = 100$ to $500 \mu\text{m}$, and from $t = 100$ to 150 s. In addition, the current 1 nA is injected at $s = 250 \mu\text{m}$ from $t = 133$ to 136 s. The dash-dot curve with diamond data points is from $\text{SK}_{\text{Ca}}/\text{IK}_{\text{Ca}}$ channels blocked and the EC tube uniformly superfused. **b** The spatial distribution of V_m at $t = 101, 120, 134$ s with a local ACh infusion, represented by solid, dashed, and dotted curves, respectively

Figure 5 shows the electrical length constant λ versus the infused ACh concentration. This parameter was obtained from ΔV_m at $s = 50, 500, 1000,$ and $1500 \mu\text{m}$ similar to the data in Fig. 3c. We observed opposite trends depending on the spatial range of the infused ACh. When the ACh is locally infused, the electrical length constant has increased about 35% with ACh up to $6 \mu\text{M}$, but λ gets short to about 50% when ACh is globally perfused (Fig. 5a). Blocking SK_{Ca} and IK_{Ca} channels suppresses the attenuated electrical propagation (turning less sensitive as shown by the changes from solid to dash-dot profile in Fig. 5a).

Electrical signal propagation in the model capillary network Next, to realize the electrical signal propagation in microvascular networks, we observed ascending hyperpolarization on a model network with each segment $500 \mu\text{m}$ (Fig. 6). This length scale is intended to consider the single-cell size of skeletal muscles and cardiac myocytes for the capillary perfusion to the tissue constituted with those cells. In the whole simulation, ACh $6 \mu\text{M}$ is locally infused in the region of a bifurcation node, as indicated in the panel (a). A local current -5 nA is injected at a position indicated in the panel (b) from $t = 20$ to 28 s. The panels (a) and (b) show the spatial distribution of V_m at $t = 20$ and 28 sec. The panel (a) shows the spreading hyperpolarization from the locally infused ACh, and the panel (b) demonstrates further hyperpolarization to upstream branches from the injected current. Panels (c) and (d) show the spatial distribution of $[\text{Ca}^{2+}]_{\text{in}}$ at $t = 20$ and 28 s. The panel (c) shows the local elevation of calcium level from the locally infused ACh. The panel (d) illustrates the calcium wave propagated to the upstream with the injected current by hyperpolarization.

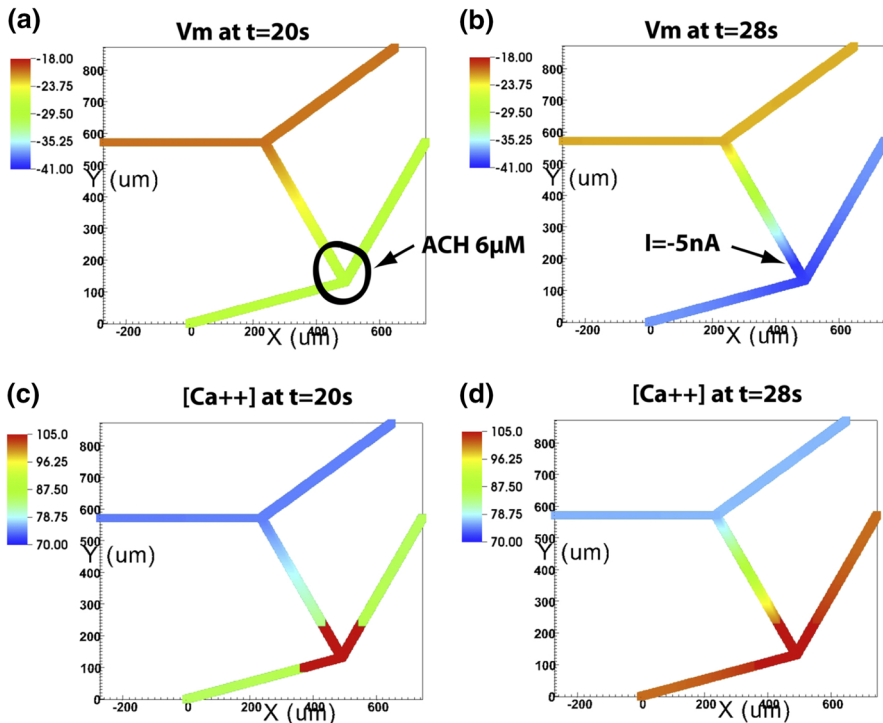


Fig. 6 Propagation of hyperpolarization in a capillary model network. **a** During the whole simulation, ACh $6 \mu\text{M}$ is infused in a local zone of the bifurcation node indicated by an arrow. **b** The current -5 nA is injected at a position within the local zone of **a** from $t = 20$ to 28 s . Panels **a** and **b** show the spatial distribution of V_m at $t = 20$ and 28 s ; the propagated hyperpolarization from the locally infused ACh, and further hyperpolarization from the injected current to the upstream, respectively. **c** and **d** The spatial distributions of $[\text{Ca}^{2+}]_{\text{in}}$ at $t = 20$ and 28 s ; the local elevation of calcium level from the locally infused ACh, and the calcium wave propagation to the upstream with hyperpolarization, respectively

The influence of acetylcholine on ascending vasodilation We investigate the influence of local infusion of ACh in the terminal area of the EC tube, and how the pre-capillary arteriole responds in vasodilation. ACh is applied in the amount of 6, 9, 12, 18, and $24 \mu\text{M}$ at the downstream from 1500 to 2000 μm . The peak of the dilatatory response of the lumped arteriole is shown in Fig. 7a. Interestingly, there is a biphasic profile in the maximum response from the local ACh infusion, with the maximum vasodilation of about 17% with ACh $12 \mu\text{M}$, comparable to the experiments in Doyle and Duling (1997). The relaxation time from the dilation to a resting state gets short from about 500 s (ACh $6 \mu\text{M}$) to 30 s (ACh $24 \mu\text{M}$).

The influence of oxygen tension and plasma ATP on ascending vasodilation Finally, we characterize the influence of oxygen consumption and induced oxygen tension to increase ATP release from the erythrocytes and its binding to EC and ascending vasodilation. We have prescribed the baseline oxygen consumption M_0 with $30 \mu\text{L} \cdot \text{O}_2/\text{g}/\text{min}$, and considered two conditions of M with 80 or $270 \mu\text{L} \cdot \text{O}_2/\text{g}/\text{min}$.

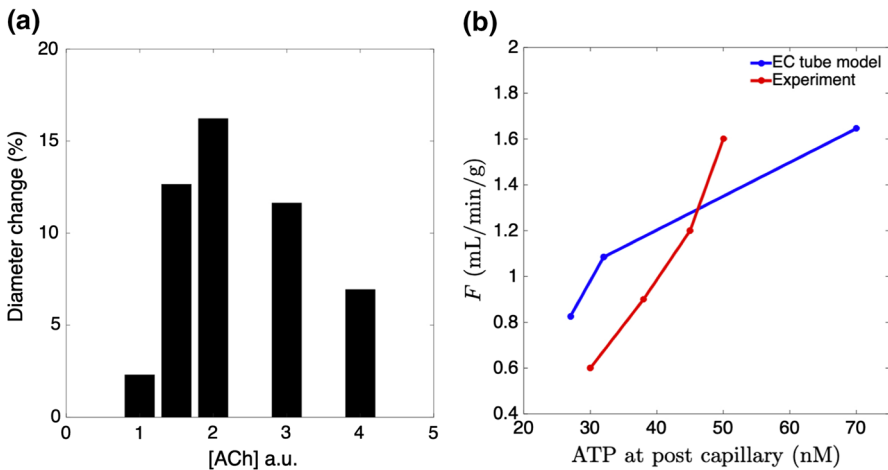


Fig. 7 **a** The maximum vasodilatory increase versus locally infused amounts of ACh. ACh is applied in the amount of 6, 9, 12, 18, and 24 μM at the downstream from 1500 to 2000 μm in the EC tube. The diameter change is with respect to the steady-state without ACh infusion. **b** Blood flow density versus plasma ATP with the changes in oxygen consumption rate. Plasma ATP at the post-capillary domain versus pre-capillary blood flow density. The EC tube model of ascending vasodilation is compared with the data of coronary blood flow regulation (Farias et al. 2005)

Figure 8a shows the membrane voltage distribution of the EC tube. With the oxygen consumption increase, the plasma ATP level has risen (Fig. 8e). Through purinergic signaling, the cytosolic calcium level is also elevated from increased purinergic IP_3 generation and calcium release from ER (Fig. 8c). Finally, from calcium-activated potassium channels, the membrane voltage is more hyperpolarized (Fig. 8a). Figure 8(b), (d), and (f) demonstrates the oscillation of membrane voltage, cytosolic calcium concentration at the terminal downstream with the increased oxygen consumption. We have observed acute surges in calcium and plasma ATP levels and relaxation by vasodilation in the simulated states of elevated oxygen consumption (Fig. 8d, f). The trend of plasma ATP is nonlinear in terms of M as shown with α term of Eq. (14). The purinergic responses of the electrophysiology of EC (V_m and $[\text{Ca}^{2+}]_{\text{in}}$) are accordingly nonlinear.

Figure 9 illustrates the time courses of electrophysiology from the SMC in the arteriole and vasodilation. When the downstream oxygen consumption is surged from $M = 80$ to 270 $\mu\text{L} \cdot \text{O}_2/\text{g}/\text{min}$, the hyperpolarized endothelial membrane voltage is propagated to the upstream. It decreases the cytosolic calcium concentration of the SMC in the arteriole (Fig. 9a). The smooth muscle in the upstream arteriole shows oscillatory profiles in IP_3 , calcium concentrations, and membrane voltage with the oscillatory period around 25 s. During 100 s after M has increased to 270 $\mu\text{L} \cdot \text{O}_2/\text{g}/\text{min}$, the capillary domain gets more oxygenated, and the plasma ATP level has gradually decreased, recovering the resting state by vasodilatory motions. Figure 7b shows the plasma ATP level at the post-capillary domain versus pre-capillary blood flow density in terms of the oxygen consumption rate. This is compared with the data of coronary blood flow regulation (Farias et al. 2005). In the experiment, the myocardial oxygen

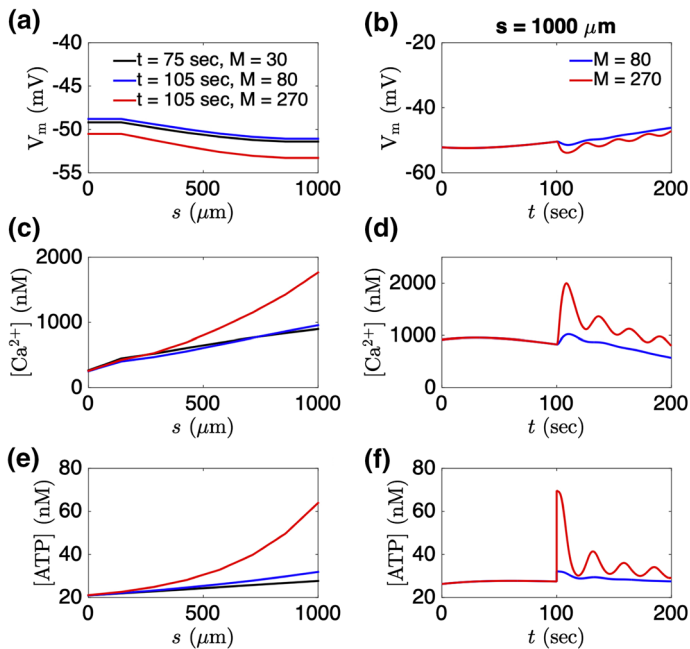


Fig. 8 Endothelial oxygen sensing dependent on the oxygen consumption rate M . **a** The membrane voltage distribution along the EC tube. **b** Time course of the EC membrane voltage at $s = 1000 \mu\text{m}$. With the elevation of oxygen consumption, the membrane is hyperpolarized and relaxes while oscillating. **c** The cytosolic calcium concentration distribution along the EC tube. **d** Time course of the cytosolic calcium concentration at $s = 1000 \mu\text{m}$. With the elevation of oxygen consumption, the cytosolic calcium level is elevated by the increased purinergic IP_3 generation and calcium release from ER. **e** and **f** The plasma ATP level has increased from a cascade of processes: elevated oxygen consumption, low oxygen tension in the post-capillary domain, and ATP release from erythrocytes. The oscillatory profiles are emerging when oxygen consumption is elevated to $270 \mu\text{L} \cdot \text{O}_2/\text{g}/\text{min}$ from $80 \mu\text{L} \cdot \text{O}_2/\text{g}/\text{min}$

consumption has increased about three times during exercise. The oxygen tension decreased from 19 to 12.9 mmHg, and coronary venous plasma ATP has increased from 31.1 to 51.2 nM. Accordingly, coronary blood flow has increased by about 2.7 times. The current model captures this trend qualitatively.

4 Discussion

The proposed mono-domain model captures the electrical propagation quantitatively along the EC tube in control and satisfies the attenuated electrical propagation from hyperpolarization. The integrated model of the EC tube and the lumped arteriole shows mechanistically upstream vasodilation responses from localized agonists of ACh or plasma ATP from erythrocytes.

Modeling NS309 stimulation and calcium dynamics The membrane depolarizes and repolarizes quickly in response to a current injection within a couple of seconds (Fig. 2). That was realized by lowering the membrane capacitance of the EC tube

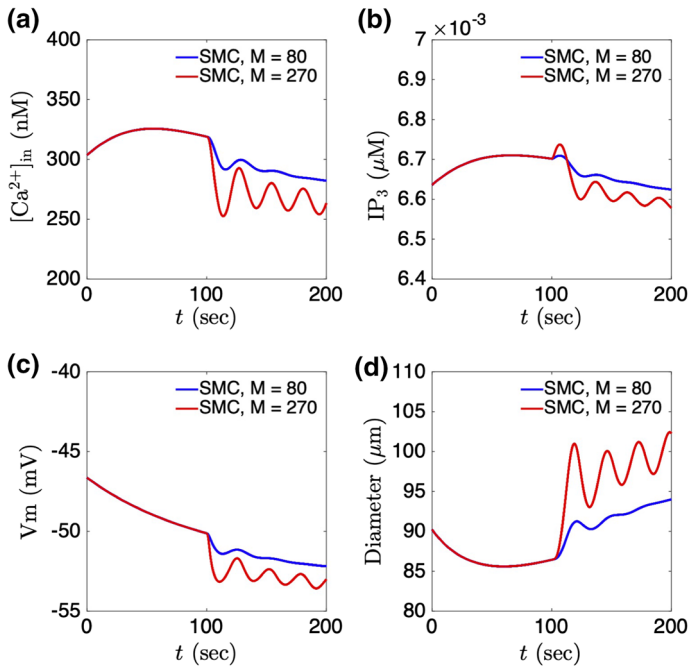


Fig. 9 Time course of the SMC electrophysiology and vasodilation in the lumped arteriole. Until $t = 100$ s, the oxygen consumption rate M is set to $30 \mu L \cdot O_2/g/min$. From $t = 100$ s, M is elevated to 80 or $270 \mu L \cdot O_2/g/min$. Enhanced oxygen consumption induces vasomotion. **a** The cytosolic calcium concentration has decreased while transitioning from a non-oscillating to an oscillating state from the increased oxygen consumption. **b** The IP_3 level has decreased while non-oscillating/oscillating from the increased M . **c** The SMC membrane is further hyperpolarized while non-oscillating/oscillating from the increased M . **d** When the tissue extracted oxygen further, the SMC is dilated without or with vasomotion for increasing the blood flow

compared to the cellular model of Silva et al. (2007). One thing that stands out is the response to NS309 stimulation. In our model, the NS309 application causes immediate hyperpolarization. However, the data show a much slower trend. We speculate that the drug is slow to get to the site of action in the experiment, possibly on the inside of the EC. The process of calmodulin domain sensitization and slow calcium-activated potassium channel activation in resting cytosolic calcium levels may account for the delay. With NS309 (and no significant increase from resting calcium levels), SK_{Ca}/IK_{Ca} activation relies upon resting calcium levels despite a substantial shift in calcium sensitivity. Presumably, this would take a very long time relative to activation via ACh (a massive increase from resting calcium) where calcium ions are readily available for SK_{Ca}/IK_{Ca} activation. However, this delay of hyperpolarization to NS309 appears to decrease with higher doses.

Application of acetylcholine locally versus globally Acetylcholine works as a vasodilator in the microvasculature, and some experiments show that the application of ACh enhances ascending hyperpolarization and increases the electrical length constant (Emerson et al. 2002). In one protocol of the current model simulations, we show

an opposite trend that ACh attenuates the electrical propagation (Fig. 5). One reason for this discrepancy is thought to be from different experiment/simulation setup. In the experiment, the perfusion of ACh is applied in a local region. On the other hand, the one specific model simulation prescribes ACh uniformly in the whole EC tube. While interrogating this opposite trend on the ACh dependency, we also simulated with a local application of ACh, and indeed, the electrical length constant has increased up to 35% with increased agonist levels from 0 to 6 μM (Fig. 5a). In the uniformly perfused ACh in the entire EC tube, more ACh evokes more hyperpolarization. The depolarization from the current injection is suppressed, working as the primary mechanism for further attenuation from higher ACh. In contrast, when ACh is infused locally, more ACh induces stronger hyperpolarization, and the membrane voltage gradient between ACh infused zone and ACh free zone gets bigger (Fig. 5b). The electrical currents increase through the ACh transitional area. The magnified membrane voltage gradient across ACh infused and ACh free zones is supposed to drive increased electrical conduction and prolonged λ from higher acetylcholine.

The simulation of the model capillary network shows the electrical and calcium signal propagation in the scale of about 1 mm, and indeed in the branched network. We have shown the propagation of hyperpolarization from the local perfusion of ACh (Fig. 6a) and highlighted ascending electrical propagation to the upstream from a local current injection (Fig. 6b). In our modeling, we did not include diffusion terms for calcium and IP_3 , i.e., the transport of calcium and IP_3 through gap junctional channels, which may somehow enhance the electrical propagation, but this is very slow in comparison to the electrical effects (Fig. 4). The calcium wave propagation in Fig. 6c, d is purely from electrical hyperpolarization.

In the current scope of this article, we do not study the influence of the number of bifurcation and density of capillary tubes with their explicit representation. However, as expressed in Eq. (14), the coronary venous plasma ATP level is proportional to the capillary volume density V_C . Therefore, higher capillary density will enhance the ascending hyperpolarization and consequently vasodilation. The bifurcation is supposed to increase the dissipation of the stimulus from the downstream (Segal and Neild 1996), and the effectiveness of ascending hyperpolarization is expected to be attenuated.

Integrated mechanistic model to support the ATP hypothesis The ATP hypothesis is about negative feedback control for balancing oxygen delivery and oxygen consumption at the local microvascular unit (Gorman et al. 2010). In the hypothesis, hemoglobin is the oxygen sensor, and red blood cells release ATP as a primary source when oxygen is unloaded from hemoglobin. The released plasma ATP then activates purinergic P2Y_1 receptors on capillary endothelial cells. This induces a retrograde conducted signal inducing vasodilation of the upstream arteriole. The proposed integrated model supports the ATP hypothesis mechanistically. In the original ATP hypothesis, ATP is broken down by nucleotidases in the plasma and on the surface of endothelial cells to ADP, AMP, and adenosine. ADP and AMP also involve in the activation of ascending vasodilation, and ADP acts on red blood cells to inhibit the further release of ATP. In our minimal model considering ATP without its breakdown, we still capture the acute response of vasodilation, and it gets relaxed to the initial conditions.

Furthermore, we recapitulate vasomotion in the lumped arteriole and the corresponding oscillatory profiles in plasma ATP and calcium dynamics in the EC tube downstream. Vasomotion is associated with enhancing the perfusion and oxygenation by the blood circulation to the capillary domain in some conditions (Goldman and Popel 2001; Domeier and Segal 2007; Thorn et al. 2011; Haddock et al. 2011). In the current induction of oscillation in the arteriole and the EC tube, the oscillatory frequency is around 0.04 Hz. In the brain, low-frequency calcium oscillation related to cerebral hemodynamics is about 0.07 Hz in rat somatosensory cortex (Du et al. 2014). In the hemodynamics of skeletal muscle with local femoral pressure reduction, there comes a slow-wave flow motion with 0.025 Hz (Schmidt et al. 1992). The modeling study of renal myogenic autoregulation and vasomotor response reconstructs 0.1–0.2 Hz vasomotion based on rat afferent arteriole (Sgouralis and Layton 2012). We expect to do a more rigorous analysis for characterizing precise conditions generating vasomotion from multiple factors (Sgouralis and Layton 2012; Kapela et al. 2012; Arciero and Secomb 2012), including internal states of pressure and oxygen consumption as well as the amounts of endogenous and pharmaceutical agonists. Altogether, this is bidirectional feedback between oxygen sensing associated ATP release from erythrocytes in the downstream and vasodilatory perfusion in the upstream, mediated by ascending electrical signals in capillary networks.

Future works There remain modeling studies of the electrical propagation in realistic capillary networks, and oxygen consumption in specific tissues with specific conditions of physiological states, pathophysiological states of ischemia, hypertension, and metabolic syndrome. We can easily apply localized perfusion of acetylcholine and pharmaceutical vasodilators in the presence of diverse forms of endothelial dysfunction in the network to investigate the global therapeutic effectiveness of vasodilation and oxygenation.

Acknowledgements The author acknowledges valuable discussions with Ranjan Pradhan, Brian E. Carlson, and Daniel A. Beard. Especially the formulation of the open probability in SK_{Ca} and IK_{Ca} channels with NS309 is accredited to Ranjan Pradhan. The author also thanks Steven Segal and Erik Behringer for the experimental data and helpful discussion. This research was partially supported by U01 HL118738-01A1 and NIGMS-P50GM094503.

References

- Arciero JC, Secomb TW (2012) Spontaneous oscillation in a model for active control of microvessel diameters. *Math Med Biol* 29:163–180
- Bagher P, Segal SS (2011) Regulation of blood flow in the microcirculation: role of conducted vasodilation. *Acta Physiol* 202:271–284
- Balay S, Eijkhout V, Gropp WD, McInnes LC, Smith BF (1997) Efficient management of parallelism in object-oriented numerical software libraries. In: Arge E, Bruaset AM, Langtangen HP (eds) *Modern software tools in scientific computing*. Birkhauser Press, Boston, pp 163–202
- Balay S, Abhyankar S, Adams M-F, Brown J, Brune P, Buschelman K, Dalcin L, Dener A, Eijkhout V, Gropp WD, Karpeyev WD, Kaushik D, Knepley MG, May D-A, McInnes LC, Smith BF, Zampini S, Zhang H (2019) PETSc users manual, Technical Report, ANL-95/11 Revision 3.12, Argonne National Laboratory
- Balay S, Abhyankar S, Adams M-F, Brown J, Bruen P, Buschelman K, Dalcin L, Dener A, Eijkhout V, Gropp WD, Karpeyev D, Kaushik D, Knepley MG, McInnes LC, Mills RT, Munson T, Rupp K, Sanan P, Smith BF, Zampini S, Zhang H (2019) PETSc. <http://www.mcs.anl.gov/petsc>

- Behringer EJ, Segal SS (2012) Tuning electrical conduction along endothelial tubes of resistance arteries through Ca^{2+} -activated K^+ channels. *Circ Res* 110:1311–1321
- Bender SB, Tune JD, Borbouse L, Long X, Sturek M, Laughlin MH (2009) Altered mechanism of adenosine-induced coronary arteriolar dilation in early-stage metabolic syndrome. *Exp Biol Med* 234:683–692
- Brahler S, Kaistha A, Schmidt VJ, Wolffe SE, Busch C, Kaistha BP, Kacik M, Hasenau A-L, Grgic I, Si H, Bond CT, Adelman JP, Wulff H, de Wit C, Hoyer J, Kohler R (2009) Genetic deficit of SK3 and IK1 channels disrupts the endothelium-derived hyperpolarizing factor vasodilator pathway and causes hypertension. *Circulation* 119:2323–2332
- Carlson BE, Beard DA (2011) Mechanical control of cation channels in the myogenic response. *Am J Physiol Heart Circ Physiol* 301:H331–H343
- Chen G, Cheung DW (1992) Characterization of acetylcholine-induced membrane hyperpolarization in endothelial cells. *Circ Res* 70:257–263
- Cohen SD, Hindmarsh AC (1996) CVODE, a Stiff/Nonstiff ODE Solver in C. *Comput Phys* 10:138–143
- Communi D, Janssens R, Suarez-Huerta N, Robaye B, Boeynaems J-M (2000) Advances in signaling by extracellular nucleotides: the role and transduction mechanisms of P_2Y receptors. *Cell Signal* 12:351–360
- Diep HK, Vigmond EJ, Segal SS, Welsh DG (2005) Defining electrical communication in skeletal muscle resistance arteries: a computational approach. *J Physiol* 568:267–281
- Domeier TL, Segal SS (2007) Electromechanical and pharmacomechanical signaling pathways for conducted vasodilatation along endothelium of hamster feed arteries. *J Physiol* 579:175–186
- Doyle MP, Duling BR (1997) Acetylcholine induces conducted vasodilation by nitric oxide-dependent and independent mechanisms. *Am J Physiol Heart Circ Physiol* 272:H1364–H1371
- Du C, Volkow ND, Koretsky AP, Pan Y (2014) Low-frequency calcium oscillations accompany deoxyhemoglobin oscillations in rat somatosensory cortex. *PNAS* 111:E4677–4686
- Duncker DJ, Bache RJ (2008) Regulation of coronary blood flow during exercise. *Physiol Rev* 88:1009–1086
- Ellsworth ML (2000) The red blood cell as an oxygen sensor: What is the evidence? *Acta Physiol Scand* 168:551–559
- Emerson GG, Neild TO, Segal SS (2002) Conduction of hyperpolarization along hamster feed arteries: augmentation by acetylcholine. *Am J Physiol Heart Circ Physiol* 283:H102–H109
- Farias M III, Gorman MW, Savage MV, Feigl EO (2005) Plasma ATP during exercise: possible role in regulation of coronary blood flow. *Am J Physiol Heart Circ Physiol* 288:H1586–H1590
- Feigl EO (1998) Neural control of coronary blood flow. *J Vasc Res* 35:85–92
- Fitzgerald SM, Kemp-Harper BK, Tare M, Parkington HC (2005) Role of endothelium-derived hyperpolarizing factor in endothelial dysfunction during diabetes. *Clin Exp Pharmacol Physiol* 32:482–487
- Goldman D, Popel AS (2001) A computational study of the effect of vasomotion on oxygen transport from capillary networks. *J Theo Biol* 209:189–199
- Gorman MW, Rooke GA, Savage MV, Jayasekara MPS, Jacobson KA, Feigl EO (2010) Adenine nucleotide control of coronary blood flow during exercise. *Am J Physiol Heart Circ Physiol* 299:H1981–H1989
- Goto K, Fujii K, Kansui Y, Abe I, Iida M (2002) Critical role of gap junctions in endothelium-dependent hyperpolarization in rat mesenteric arteries. *Clin Exp Pharmacol Physiol* 29:595–602
- Haddock RE, Grayson TH, Morris MJ, Howitt L, Chadha PS, Sandow SL (2011) Diet-induced obesity impairs endothelium-derived hyperpolarization via altered potassium channel signaling mechanisms. *PLoS ONE* 6:e16423
- Hai C-M, Murphy RA (1988) Cross-bridge phosphorylation and regulation of latch state in smooth muscle. *Am J Physiol* 254:C99–C106
- Ito Y, Kitamura K, Kuriyama H (1980) Nitroglycerine and catecholamine actions on smooth muscle cells of the canine coronary artery. *J Physiol* 309:171–183
- Kapela A, Bezerianos A, Tsoukias NM (2008) A mathematical model of Ca^{2+} dynamics in rat mesenteric smooth muscle cell: agonist and NO stimulation. *J Theor Biol* 253:238–260
- Kapela A, Bezerianos A, Tsoukias NM (2009) A mathematical model of vasoreactivity in rat mesenteric arterioles: I. Myoendothelial communication. *Microcirculation* 16:694–713
- Kapela A, Parikh J, Tsoukias NM (2012) Multiple factors influence calcium synchronization in arterial vasomotion. *Biophys J* 102:211–220
- Kuo L, Davis MJ, Chilian WM (1990) Endothelium-dependent, flow-induced dilation of isolated coronary arterioles. *Am J Physiol* 259:H1063–H1070

- Park Y, Capobianco S, Gao X, Falck JR, Dellsperger KC, Zhang C (2008) Role of EDHF in type 2 diabetes-induced endothelial dysfunction. *Am J Physiol Heart Circ Physiol* 295:H1982–1988
- Pradhan RK, Feigl EO, Gorman MW, Brengelmann GL, Beard DA (2016) Open-loop (feed-forward) and feedback control of coronary blood flow during exercise, cardiac pacing, and pressure changes. *Am J Physiol Heart Circ Physiol* 310:H1683–1694
- Raqeeb A, Sheng J, Ao N, Braun AP (2011) Purinergic P₂Y₂ receptors mediate rapid Ca²⁺ mobilization, membrane hyperpolarization and nitric oxide production in human vascular endothelial cells. *Cell Calcium* 49:240–248
- Schmidt JA, Intaglietta M, Borgstrom P (1992) Periodic hemodynamics in skeletal muscle during local arterial pressure reduction. *J Appl Physiol* 73:1077–1083
- Schmidt VJ, Wolffe SE, Boettcher M, de Wit C (2008) Gap junctions synchronize vascular tone within the microcirculation. *Pharmacol Rep* 60:68–74
- Segal SS, Duling BR (1986) Flow control among microvessels coordinated by intercellular conduction. *Science* 234:868–870
- Segal S, Neild TO (1996) Conducted depolarization in arteriole networks of the guinea-pig small intestine: effect of branching on signal dissipation. *J Physiol* 496:229–244
- Sgouralis I, Layton AT (2012) Autoregulation and conduction of vasomotor responses in a mathematical model of the rat afferent arteriole. *Am J Physiol Renal Physiol* 303:F229–F239
- Silva HS, Kapela A, Tsoukias NM (2007) A mathematical model of plasma membrane electrophysiology and calcium dynamics in vascular endothelial cells. *Am J Physiol Cell Physiol* 293:C277–C293
- Stankevicius E, Dalsgaard T, Kroigaard C, Beck L, Boedtkjer E, Misfeldt MW, Nielsen G, Schjorring O, Hughes A, Simonsen U (2011) Opening of small and intermediate calcium-activated potassium channels induces relaxation mainly mediated by nitric-oxide release in large arteries and endothelium-derived hyperpolarizing factor in small arteries from rat. *J Pharmacol Exp Therap* 339:842–850
- Thorn CE, Kyte H, Slaff DW, Shore AC (2011) An association between vasomotion and oxygen extraction. *Am J Physiol Heart Circ Physiol* 301:H442–H449

Publisher's Note Springer Nature remains neutral with regard to jurisdictional claims in published maps and institutional affiliations.